Inorg. Chem. **2007**, *46*, 1617−1626

Synthesis, Structure, and Redox Properties of N-Confused Bis(porphyrinatonickel(II)) Linked by *o*-Xylene

Piotr J. Chmielewski*

Department of Chemistry, University of Wroclaw, 14 F. Joliot-Curie Street, 50-383 Wroclaw, Poland

Received September 21, 2006

In a reaction of 5,10,15,20-tetraaryl-2-aza-21-carbaporphyrinato nickel(II) **2** with α,α′-dibromo-*o*-xylene, three different complexes containing a xylene moiety were obtained in the presence of a proton scavenger. The products were characterized by mass spectrometry, UV–vis, NMR, and, in the case of the dimeric complex **3**, X-ray crystallographic analysis (space group $P\bar{1}$, a =16.455(3) Å, b = 16.776(3) Å, c = 18.400(4) Å, α = 77.43(3)°, β = 75.31(3)°, γ = 66.20(3)°, V = 4457.1(19) Å^3, Z = 2). The monomeric species, diamagnetic **4** and paramagnetic **5**, contain one and two bromoxylene residues, respectively, while in **3**, the xylene bridge links two macrocyclic subunits, involving their internal carbons (C21) coordinated to diamagnetic nickel(II). Cyclovoltammetric measurements for *o*-xylene-linked bis(carbaporphyrinoid) **3** indicate cooperative effects resulting from an interaction between the subunits despite the isolation of their aromatic π-bond systems. An EPR-controlled titration of **3** with bromine allows consecutive detection of the mono- and bis-oxidized species (**3**Br, **3**Br$_2$). The spectral patterns and spin-Hamiltonian parameters indicate metal-centered oxidation in **3**Br (g_x = 2.358, g_y = 2.150, g_z = 2.062, A_x^{Br} = 15, A_y^{Br} = 35, A_z^{Br} = 129 G) and interaction of two electron spins of nickel(III) ions in **3**Br$_2$ (g_x = 2.328, g_y = 2.195, g_z = 2.065, D = 0.0173 cm^{-1}, E = –0.0018 cm^{-1}, A_z^{Br} = 63 G). A product of the chemical reduction of a protonated form of the dimer was also detected by means of EPR (g_1 = 2.298, g_2 = 2.218, g_3 = 2.192), although no interaction between the nickel(I) centers can be observed for the reduced species.

Introduction

Since its discovery in 1994, N-confused (inverted) porphyrin NCP, 5,10,15,20-tetraaryl-2-aza-21-carbaporphyrin **1**[1−3] has continued to attract attention because of its remarkable tendency to form a variety of rare organometallic compounds,[4−12] multimodal coordination properties,[11−24] and peculiar reactivity of metal complexes.[25−36] The alterations of optical, acid−base, coordination, and redox properties of the macrocycle allow fine-tuning or profound variation of the properties of the complex. The special character of the *confused* pyrrole is reflected by its susceptibility to various types of reaction, also in the free-base porphyrin, that lead to the formation of many derivatives bearing substituents

* E-mail: pjc@wchuwr.chem.uni.wroc.pl.

(1) Chmielewski, P. J.; Latos-Grażyński, L.; Rachlewicz, K.; Glowiak, T. *Angew. Chem., Int. Ed. Engl.* **1994**, *33*, 779−781.
(2) Furuta, H.; Asano, T.; Ogawa, T. *J. Am. Chem. Soc.* **1994**, *116*, 767.
(3) Geier, G. R., III; Haynes, D. M.; Lindsey, J. S. *Org. Lett.* **1999**, *1*, 1455.
(4) Furuta, H.; Ogawa, T.; Uwatoko, Y.; Araki, K. *Inorg. Chem.* **1999**, *38*, 2676.
(5) Ogawa, T.; Furuta, H.; Takahashi, M.; Morino, A.; Uno, H. *J. Organomet. Chem.* **2000**, *611*, 551.
(6) Maeda, H.; Ishikawa, Y.; Matsueda, H.; Osuka, A.; Furuta, H. *J. Am. Chem. Soc.* **2003**, *125*, 11822.
(7) Maeda, H.; Osuka, A.; Ishikawa, Y.; Aritome, I.; Hisaeda, Y.; Furuta, H. *Org. Lett.* **2003**, *5*, 1293.
(8) Liu, J.-C.; Ishizuka, T.; Osuka, A.; Furuta, H. *Chem. Commun.* **2004**, 1908.
(9) Chmielewski, P. J.; Latos-Grażyński, L. *Inorg. Chem.* **1997**, *36*, 840.
(10) Chmielewski, P. J.; Latos-Grażyński, L.; Schmidt, I. *Inorg. Chem.* **2000**, *39*, 5475.
(11) Harvey, J. D.; Ziegler, C. J. *Chem. Commun.* **2002**, 1942.
(12) Harvey, J. D.; Ziegler, C. J. *Chem. Commun.* **2004**, 1666.
(13) Harvey, J. D.; Ziegler, C. J. *Coord. Chem. Rev.* **2003**, *247*, 1.
(14) Chmielewski, P. J.; Latos-Grażyński, L. *Coord. Chem. Rev.* **2005**, *249*, 2510.
(15) Furuta, H.; Kubo, N.; Maeda, H.; Ishizuka, T.; Osuka, A.; Nanami, H.; Ogawa, T. *Inorg. Chem.* **2000**, *39*, 5424.
(16) Srinivasan, A.; Furuta, H.; Osuka, A. *Chem. Commun.* **2001**, 1666.
(17) Furuta, H.; Maeda, H.; Osuka, A. *Chem. Commun.* **2002**, 1795.
(18) Furuta, H.; Ishizuka, T.; Osuka, A. *J. Am. Chem. Soc.* **2002**, *124*, 5622.
(19) Furuta, H.; Youfu, K.; Maeda, H.; Osuka, A. *Angew. Chem., Int. Ed.* **2003**, *42*, 2186.
(20) Furuta, H.; Morimoto, T.; Osuka, A. *Inorg. Chem.* **2004**, *43*, 1618.
(21) Chen, W.-C.; Hung, C.-H. *Inorg. Chem.* **2001**, *40*, 5070.
(22) Hung, C.-H.; Chen, W.-C.; Lee, G.-H.; Peng, S.-M. *Chem. Commun.* **2002**, 1516.
(23) Rachlewicz, K.; Wang, S.-L.; Peng, C.-H.; Hung, C.-H.; Latos-Grażyński, L. *Inorg. Chem.* **2003**, *42*, 7348−7350.

10.1021/ic061793e CCC: $37.00
Published on Web 02/02/2007

Chart 1

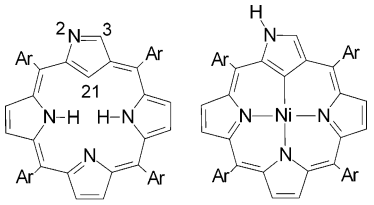

1 **2**

on the external nitrogen (N2),[37−40] external carbon (C3),[41−43] or internal carbon (C21).[44,45] A facile modification of these properties makes **1** a potentially attractive "replacement" of regular porphyrins in molecular[46,47] and supramolecular systems[48−52] as long as the aromatic character of the macrocycle is retained. A built-in external coordinating site of **1** or some of its derivatives, that is, the exposed outer nitrogen of the *confused* pyrrole, has been shown to be involved in the formation of the coordinatively linked oligomers.[15,18−20,22,33,53,54] Also, a number of covalent dimers consisting of N-confused porphyrin subunits linked either directly[43,55] or by an alkanyl bridge[27,29,38] have been reported recently.The present contribution is focused on the synthesis and characterization of N-confused porphyrin nickel complexes comprising an *o*-xylene fragment. One of these complexes consists of two porphyrinoid subunits covalently linked by such a semirigid bridge. We show here that these subunits interact despite the lack of coupling between the π-electron systems, which is reflected by the redox and spectroscopic properties of the dimer.

Scheme 1

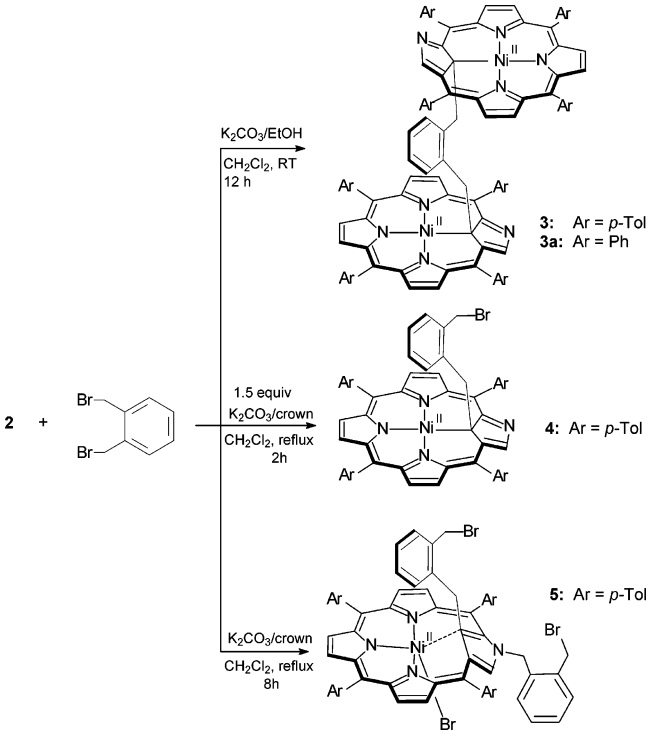

Results and Discussion

Synthesis and Characterization. Complexes **3**−**5** can be obtained by combining the NCP nickel(II) complex **2** with 1,2-bis(bromomethyl)benzene ($XylBr_2$), depending on the reaction conditions (Scheme 1). Several factors, such as excess of the alkylation agent, type of proton scavenger applied, and reaction temperature, influence the relative yield of 2- or 21-substituted products. Similar effects have been observed previously for mono- or dihaloalkanes.[27,28] In the case of $XylBr_2$, however, the reaction with **2** can be optimized either with respect to the dimer **3** or to the systems comprising one (**4**) or two (**5**) 2-(bromomethyl)benzyl groups (Scheme 1). Although known as being a reactive electrophile,[38] the bromobenzyl group remains intact under the present reaction conditions and with the applied separation methods, except for the relatively slow formation of the dimer **3**. It makes monomeric systems **4** and **5** readily obtainable and promising intermediates for the construction of bigger molecular assemblies containing the N-confused porphyrin fragment and *o*-xylene bridges. The mass spectra of complexes **3**, **4**, and **5** (m/z = 1556.8, 911.2, and 1174.1 amu, respectively) are in agreement with their compositions.

The optical spectra of **3** and **4** (Figure 1) are almost identical except for the molar extinction coefficients which are about twice as high for each of the bands in the spectrum

(24) Toganoh, M.; Konagawa, J.; Furuta, H. *Inorg. Chem.* **2006**, *45*, 3852.
(25) Chmielewski, P. J.; Latos-Grażyński, L.; Glowiak, T. *J. Am. Chem. Soc.* **1996**, *118*, 5690.
(26) Chmielewski, P. J.; Latos-Grażyński, L. *Inorg. Chem.* **2000**, *39*, 5639.
(27) Schmidt, I.; Chmielewski, P. J.; Ciunik, Z. *J. Org. Chem.* **2002**, *67*, 8917.
(28) Schmidt, I.; Chmielewski, P. J. *Inorg. Chem.* **2003**, *42*, 5579.
(29) Schmidt, I.; Chmielewski, P. J. *Chem. Commun.* **2002**, 92.
(30) Xiao, Z.; Patrick, B. O.; Dolphin, D. *Chem. Commun.* **2002**, 1816.
(31) Xiao, Z.; Patrick, B. O.; Dolphin, D. *Chem. Commun.* **2003**, 1062.
(32) Xiao, Z.; Patrick, B. O.; Dolphin, D. *Inorg. Chem.* **2003**, *42*, 8125.
(33) Rachlewicz, K.; Wang, S.-L.; Ko, J.-L.; Hung, C.-H.; Latos-Grażyński, L. *J. Am. Chem. Soc.* **2004**, *126*, 4420−4431.
(34) Bohle, D. S.; Chen, W.-C.; Hung, C.-H. *Inorg. Chem.* **2002**, *41*, 3334.
(35) Hung, C.-H.; Wang, S.-L.; Ko, J.-L.; Peng, C.-H.; Hu, C.-H.; Lee, M.-T. *Org. Lett.* **2004**, *6*, 1393.
(36) Furuta, H.; Maeda, H.; Osuka, A. *Org. Lett.* **2002**, *4*, 181.
(37) Chmielewski, P. J.; Latos-Grażyński, L. *J. Chem. Soc., Perkin Trans. 2* **1995**, 503.
(38) Chmielewski, P. J. *Org. Lett.* **2005**, *7*, 1789.
(39) Qu, W.; Ding, T.; Cetin, A.; Harvey, J. D.; Taschner, M. J.; Ziegler, C. J. *J. Org. Chem.* **2006**, *71*, 811.
(40) Li, X.; Chmielewski, P. J.; Xiang, J.; Xu, J.; Li, Y.; Liu, H.; Zhu, D. *Org. Lett.* **2006**, *8*, 1137.
(41) Schmidt, I.; Chmielewski, P. J. *Tetrahedron Lett.* **2001**, *42*, 1151.
(42) Schmidt, I.; Chmielewski, P. J. *Tetrahedron Lett.* **2001**, *42*, 6389.
(43) Chmielewski, P. J. *Angew. Chem., Int. Ed.* **2004**, *43*, 5655.
(44) Ishikawa, Y.; Yoshida, I.; Akaiwa, K.; Koguchi, E.; Sasaki, T.; Furuta, H. *Chem. Lett.* **1997**, 453.
(45) Furuta, H.; Ishizuka, T.; Osuka, A.; Ogawa, T. *J. Am. Chem. Soc.* **1999**, *121*, 2945.
(46) Wojaczyński, J.; Latos-Grażyński, L. *Coord. Chem. Rev.* **2000**, *204*, 113.
(47) Burrell, A.; Officer, D. L.; Plieger, P. G.; Reid, D. C. W. *Chem. Rev.* **2001**, *101*, 2751.
(48) Atwood, J. L.; Davies, J. E.; MacNicol, D. D.; Vogtle, F. E. *Comprehensive Supramolecular Chemistry*; Pergamon: Oxford, U.K., 1996.
(49) Hung, C.-H.; Chang, C.-S.; Ching, W.-M.; Chuang, C.-H. *Chem. Commun.* 2006, 1866.
(50) Lehn, J.-M. *Supramolecular Chemistry*: *Concepts and Perspectives*; WCH: Wenheim, Germany, 1995.
(51) Wasielewski, M. R. *Chem. Rev.* **1992**, *92*, 435.
(52) D'Souza, F.; Smith, P. M.; Rogers, L.; Zandler, M. E.; Islam, D.-M. S.; Araki, Y.; Ito, O. *Inorg. Chem.* **2006**, *45*, 5057.
(53) Chmielewski, P. J.; Schmidt, I. *Inorg. Chem.* **2004**, *43*, 1885.
(54) Chmielewski, P. J. *Angew. Chem., Int. Ed.* **2005**, *44*, 6417.
(55) Ishizuka, T.; Osuka, A.; Furuta, H. *Angew. Chem., Int. Ed.* **2004**, *43*, 5077.

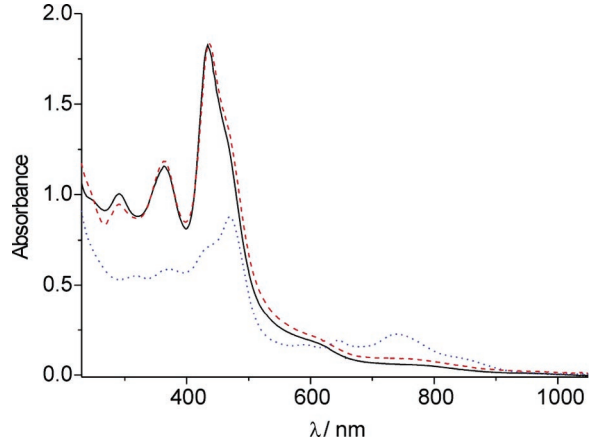

Figure 1. Optical spectra (CH_2Cl_2) of **3** (black solid line), **4** (red dashed), and **5** (blue dotted).

of the dimeric complex than those of the monomeric species. That reflects the identity of chromophores in these systems and lack of conjugation between the aromatic subunits in the dimeric system **3**, which would lead to a vibronic splitting of the Soret-type band at 434 nm.[43] On the other hand, the spectral features observed for **5**, that is, a significant decrease of the Soret-like band and increase of the band intensities at higher wavelengths, are related to a reduction of the aromatic character of the system.

^{1}H and ^{13}C NMR spectroscopy, including homo- and heteronuclear 2D techniques, were applied for the characterization of the new compounds. The low symmetry of **1** and its derivatives makes their NMR spectra complicated but rich in structural information, sometimes allowing observation of a unique signal for each proton.[27,29,38,53] Because of their aromatic character, the close distance between porphyrinoid subunits as well as their arrangement can be recognized on the basis of characteristic up- or downfield shift of particular proton signals caused by the macrocyclic ring current.

In the Figure 2, the effect of proximity of two aromatic macrocyclic rings in **3** is clearly seen as a strong upfield shift (2 ppm) of signals of the diastereotopic methylene protons of the xylene fragment (21-CH_2) with respect to that in the monomeric complex **4**. Also the signal of H3, that is, the proton bound to the external carbon C3 of the *confused* pyrrole, and those of the β-pyrrole protons in the ^{1}H NMR spectrum of **3** are shifted to lower frequencies relative to those observed for **4**. The synergetic effect of two ring currents indicates an eclipsed arrangement of the porphyrinoid subunits. The spectrum of **3** or **3a** consists of two sets of signals of the same intensity which is accounted for by a presence of a pair of diastereomers. It is particularly well demonstrated by the presence of four doublets of the diastereotopic methylene protons in the high-field region around −3 ppm. Also, in the case of **3**, eight signals of methyl groups of the *meso*-tolyl substituents occur in the region of 2.9−2.3 ppm. Although the molecule of dimer possesses an effective twofold symmetry, each of the two coordinated sp^3 carbons of the confused pyrrole (C21) constitutes a stereogenic center. Thus, two NMR-distinguishable stereoisomers can be observed: a pair of RR and SS

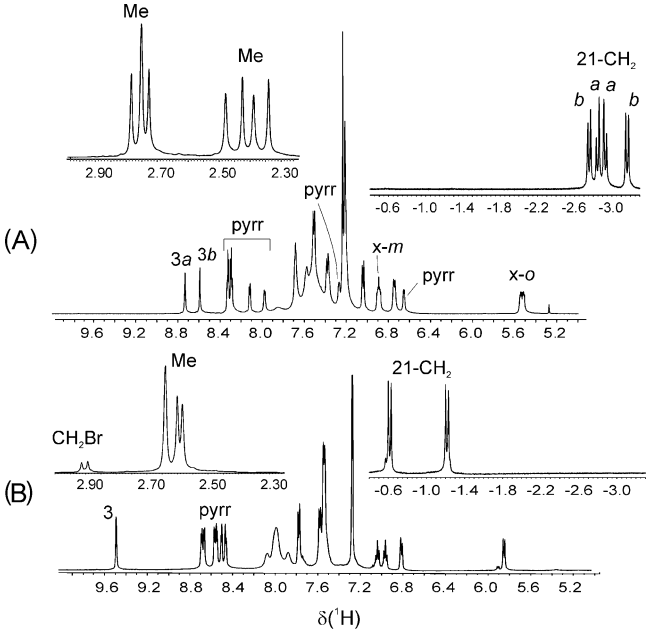

Figure 2. ^{1}H NMR spectra (500 MHz, $CDCl_3$, 298 K) of **3** (trace A) and **4** (trace B). The assignments are as follows: pyrr = β-pyrrole, Me = para-methyl groups of meso-tolyl substituents, 21-CH_2 = diastereotopic methylene groups bound to the internal carbon (the a and b indices are introduced to distinguish diastereomers), CH_2Br = one of the signals of diastereotopic bromomethyl group (the other is obscured by Me signals), 3, 3a, and 3b = protons on the external carbon of the confused pyrrole in **4** and in diastereomers of **3**; x-*o*, x-*m* = phenylene ortho and meta protons of the xylene bridge.

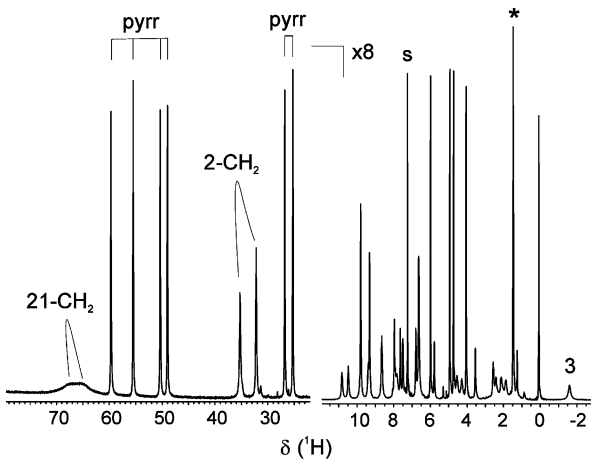

Figure 3. ^{1}H NMR spectrum of **5** (500 MHz, 3, 298 K). The assignments are as follows: pyrr = β-pyrrole protons, 21-CH_2 and 2-CH_2 = methylene protons of the substituents attached to the internal carbon and external nitrogen of the confused pyrrole, respectively, 3 = proton on the external nitrogen of the confused pyrrole, s = solvent. The signal of water dissolved in $CDCl_3$ is marked with asterisk.

enantiomers and an achiral RS meso form. In the ^{1}H−^{13}C HMBC experiments (**3a**, $CDCl_3$, 298 K), protons H3 and the diastereotopic methylene 21-CH_2 correlate with carbon C21 at 39.4 (diastereomer a) and 39.6 ppm (diastereomer b), that is, in the region typical for sp^3 carbons. That indicates similarity of the coordination core structure of **3** or **3a** to other 21-alkylated nickel(II) complexes.[25,27,28,29,53]

The ^{1}H NMR spectrum of **5** (Figure 3) reveals the paramagnetic character of the 2,21-bis(bromoxylene)-substituted system. The triplet ground state of the nickel(II) ion is caused by changes in the coordination properties of

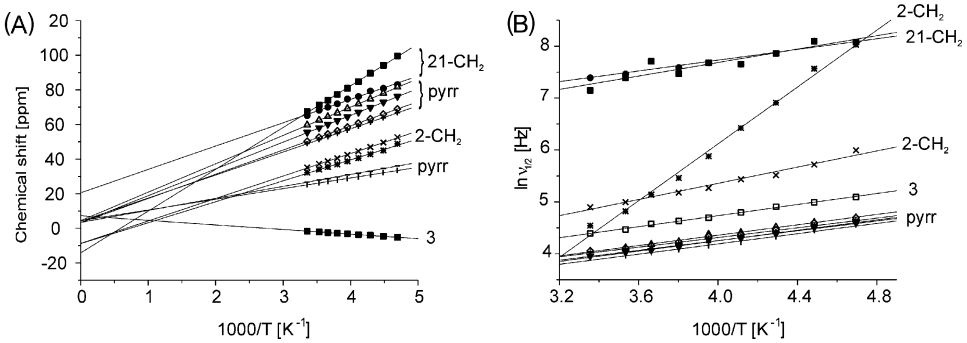

Figure 4. Dependencies of chemical shifts (A) and of logarithms of ^{1}H NMR line half-widths (B) on reciprocal temperature for pyrrole and methylene protons of **5**.

the macrocycle in **5** which has character of a monoanionic tridentate ligand with only weak side-on interaction of C21 with metal center.[25] The spectrum resembles those of nickel(II) complexes of 2,21-dimethylated or 2-protonated-21-alkylated derivatives of **1**[25,28] with strong downfield shifts of the β-pyrrole signals (25−60 ppm), upfield shift of the signal of proton 3 (−1.7 ppm), and strong broadening of signals of the fragment directly bonded to the internal carbon (21-CH_2). The methylene protons are diastereotopic, but the differentiation of their chemical shift (about 5 ppm) is much poorer than in the case of 2-protonated-21-benzylated NCP nickel(II) chloride complex where signal separation for the 21-CH_2 fragment was close to 50 ppm at 298 K.[28]

The chemical shift temperature dependencies for pyrrole protons of **5** (Figure 4A) only slightly decline from the Curie behavior with intercepts close to the chemical shifts of diamagnetic references. On the other hand, nonzero intercepts are observed for the isotropic shifts of the methylene fragments directly connected with the macrocycle indicating some contribution of the dipolar interaction resulting from a zero-field splitting anisotropy that introduces a T^{-2}-dependent curvature.[56] This dipolar interaction along with possible conformational dynamics of the molecule seem to be also responsible for a peculiar temperature dependence of the line width $\nu_{1/2}$ of one of the methylene protons attached to the nitrogen of the confused pyrrole (2-CH_2). For nonviscous solutions, the dependencies of logarithms of $\nu_{1/2}$ versus T^{-1} are expected to be linear with the same positive slope for all protons of the given paramagnetic system.[57,58,59] As shown in Figure 4B, all but one of the dependencies of $\ln(\nu_{1/2}) = f(1/T)$ present similar slopes despite various positions and distances of protons with respect to the paramagnetic center. The exceptionally strong dependence for one proton of the diastereotopic pair could in principle be related to a temperature dependent conformational equilibrium involving rotation about a C−N bond. A nonlinear temperature dependence of signal linewidths has been observed in the case of benziporphyrin nickel(II) complexes and rationalized in terms of conformational flexibility of the system with aryl ring weakly interacting with metal ion.[60]

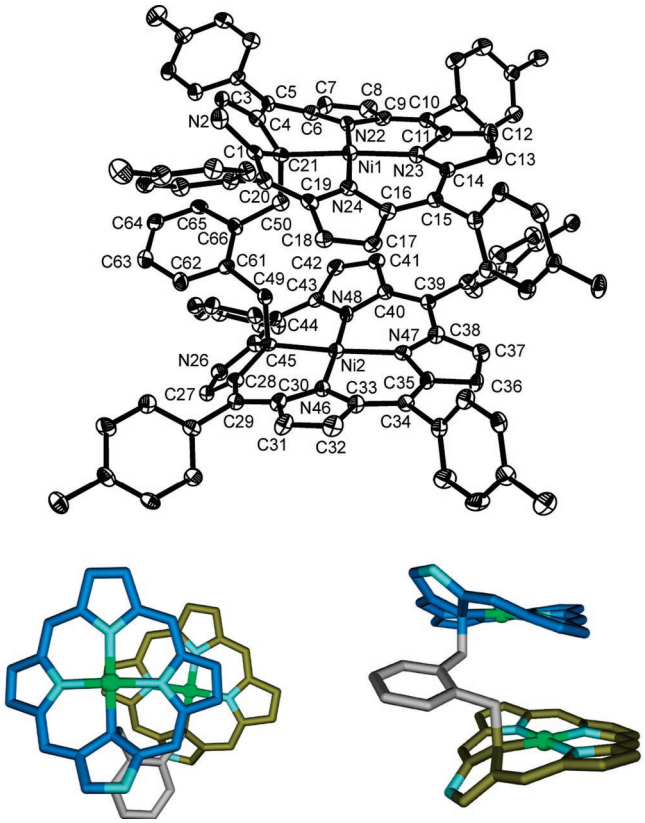

Figure 5. X-ray structure of **3**. (top) An ORTEP representation with 30% thermal ellipsoids and atom numbering scheme (all hydrogens and solvent molecules are omitted). (bottom) Two projections of wire-frame representation (all *meso*-aryl substituents are omitted for clarity) showing arrangement and distortions of the subunits. The structure presents one out of the three possible stereoisomers. The diastereomers are indistinguishable because of a C−N site disorder on the confused pyrrole.

Solid-State Characterization of 3. The X-ray structure of **3** confirms the integrity and identity of the compound and reveals a face-to-face orientation of the porphyrinoid subunits in the solid state (Figure 5). To the best of our knowledge, this is the first example of a structurally characterized bis(porphyrin) with a covalent linker that spans between the coordination systems of the macrocyclic subunits.[61] In each of the macrocyclic fragments, the nickel(II)

(56) *NMR of Paramagnetic Molecules. Principles and Applications*; La Mar, G. N., Horrocks, W. D., Jr., Holm, R. H., Eds; Academic Press: New York, 1973.
(57) Satterlee, J. D.; La, Mar, G. N.; Bold, T. J. *J. Am. Chem. Soc.* **1977**, *99*, 1088.
(58) La Mar, G. N.; Sherman, E. O. *J. Am. Chem. Soc.* **1970**, *92*, 2691.
(59) Bertini, I.; Luchinat, C. *Coord. Chem. Rev.* **1996**, *150*, 1.
(60) Stepień, M.; Latos-Grażyński, L.; Szterenberg, L. *Inorg. Chem.* **2004**, *43*, 6654.

ion is coordinated in a square-planar fashion which is in line with a diamagnetic character of **3**. Each coordination core consists of three pyrrolic nitrogens and one pyramidal carbon atom. The metal−donor distances (Å) (Ni1−C21 = 2.012-(7), Ni1−N22 = 1.944(7), Ni1−N23 = 1.957(5), Ni1−N24 = 1.946(7), Ni2−C45 = 2.018(7), Ni2−N46 = 1.943(6), Ni2−N47 = 1.958(7), Ni2−N48 = 1.955(5)) are similar to those observed for the nickel(II) complex of 21-methylated derivative of **1**.[25] Both subunits display the same saddle-shape distortion of the macrocyclic ring with the plane of the confused pyrrole tipped out of the mean plane of the macrocycle. The set of donors and the metal atom are essentially coplanar with an average displacement from the mean plane of 0.02 Å. The subunits are nearly parallel with an angle between the mean macrocyclic planes of 16° and with the dihedral angle between planes defined by the NiCNNN atom sets of only 2.6(3)°. Because of the angular character of the *o*-xylene bridge, the subunits are shifted with respect to each other, which increases the distance between metal centers to 5.77 Å. Although a mixture of diastereomers is observed by the solution NMR (Figure 2A), their presence cannot be determined in the solid-state because of the disorder of molecule. The difference in the electron density of nitrogen and carbon is too small to allow distinction between atoms that actually occupy sites N2, C3, N26, and C27. This is indicative of fourfold disorder on the confused pyrroles.

The structure of **3** is to some extent related to the cofacial metallobisporphyrins[62−64] or metallobiscorroles[65−69] except for intrinsic chirality of one of its diastereomers and rotational freedom on the bridging xylene fragment. Such a rotation, which seems to be facile in solution, allows changes in the arrangement of the macrocyclic subunits with respect to each other and with respect to the bridge.

Protonation and Redox Properties. The external nitrogen of the confused pyrrole in 21-substituted derivatives of NCP nickel(II) complexes is nucleophilic, and its protonation[25,28,29] or coordination to a metal ion[53] has been shown for a number of monomeric systems. In the dimeric complex **3**, there are two basic sites, and the process of their protonation may reflect interaction between the subunits.

Acidification of **3** by addition of chloroform saturated with gaseous hydrogen chloride leads to changes of the ground state of the nickel(II) from singlet to triplet because of concurrent coordination of the chloride to the metal ion. It is reflected by significant changes in the ^{1}H NMR spectrum with a strong paramagnetic shift of pyrrole and methylene signals similar to those observed for the monomeric systems.[25,28] Because of the fast chemical exchange at room temperature, the spectral lines are very broad, but they sharpen at lower temperatures allowing observation of the high-field shifted signal of 2-NH protons and two sets of downfield shifted β-pyrrole protons (Figure 6). The number of resonances originates from the presence of diastereomers described above for **3** rather than from the simultaneous presence of mono- and bisprotonated species since the relative intensities of signals do not vary with the amount of acid. It seems that even at low temperature the rate of exchange between mono- and bisprotonated complexes is too high to allow observation of separate signals for these species. Alternatively, the simultaneous protonation of both nitrogen sites can be taken into account, which would imply lack of any electrostatic interaction between the subunits. The dependence of the chemical shifts in the limited temperature range (253−213 K) displays Curie behavior and thus no effects are observed that could be related to an interaction of the paramagnetic centers.

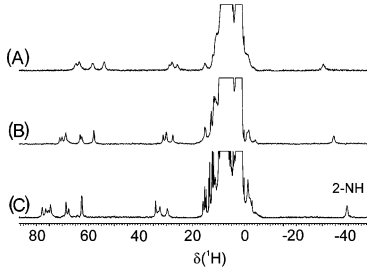

Figure 6. ^{1}H NMR spectra (500 MHz, $CDCl_3$) of [**3**$(HCl)_2$] at T = 253 (A), 233 (B), and 213 K (C).

The two-stage character of the protonation of **3** can be inferred from a spectrophotometric titration of the dimer with trifluoroacetic acid (TFAH) where spectral changes indicate consecutive formation of two species, which is dependent on acid concentration (Figure 7A). Importantly, alkalization of the solution fully reverses the spectral changes indicating that none of them is related with an acid-induced demetallation. In contrast, formation of only one protonated species is observed upon addition of TFAH to the solution of monomeric complex **4** up to 3-fold excess and further changes are attributed to the demetallation (see Supporting Information).

Oxidation of **3** with bromine was monitored by UV−vis spectrometry. The spectrophotometric titration with Br_2 indicates that the process consists of two well-separated steps (Figure 7B) suggesting presence of two redox-active sites of various oxidation potentials.

Cyclovoltammetric measurements were performed in dichloromethane using $[BuN_4]ClO_4$ supporting electrolyte and referenced against a ferrocene/ferrocenium couple as an internal standard. The representative electrochemical experiments are presented in Figure 8, and the data are collected in Table 1.

The cyclic voltammogram of **3** consists of two reduction couples separated by 150 mV and two irreversible oxidation

(61) Setsune, J.; Ito, S.; Takeda, H.; Ishimaru, Y.; Kitao, T.; Sato, M.; Ohya-Nishiguchi, H. *Organometallics* **1997**, *16*, 597.
(62) Collman, J. P.; Wagenknecht, P. S.; Hutchison, J. E. *Angew. Chem., Int. Ed. Engl.* **1994**, *33*, 1537.
(63) Chang, C. J.; Deng, Y.; Heyduk, A. F.; Chang, C. K.; Nocera, D. G. *Inorg. Chem.* **2000**, *39*, 959.
(64) Deng, Y.; Chang, C. J.; Nocera, D. G. *J. Am. Chem. Soc.* **2000**, *122*, 410.
(65) Jerome, F.; Billier, B.; Barbe, J. M.; Espinosa, E.; Dahaoui, S.; Lecomte, C.; Guilard, R. *Angew. Chem., Int. Ed. Engl.* **2000**, *39*, 4051.
(66) Guilard, R.; Gros, C. P.; Bolze, F.; Jerome, F.; Ou, Z.; Shao, J.; Fischer, J.; Weiss, R.; Kadish, K. M. *Inorg. Chem.* **2001**, *40*, 4845.
(67) Guilard, R.; Jerome, F.; Barbe, J. M.; Gros, C. P.; Ou, Z.; Shao, J.; Fischer, J.; Weiss, R.; Kadish, K. M. *Inorg. Chem.* **2001**, *40*, 4856.
(68) Jerome, F.; Barbe, J. M.; Gros, C. P.; Guilard, R.; Fischer, J.; Weiss, R. *New J. Chem.* **2001**, 93.
(69) Pacholska, E.; Espinosa, E.; Guilard, R. *Dalton Trans.* **2004,** 3181.

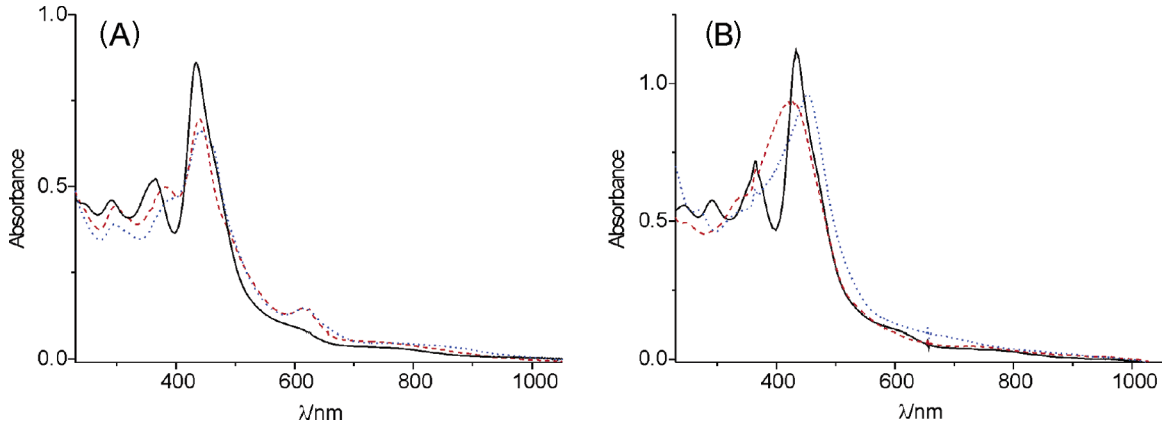

Figure 7. Selected spectra recorded upon spectrophotometric titration of **3** with TFAH (A) and with Br_2 (B). Black solid line, 0 equiv; red dashed, 1.2 equiv; blue dotted, 4 equiv.

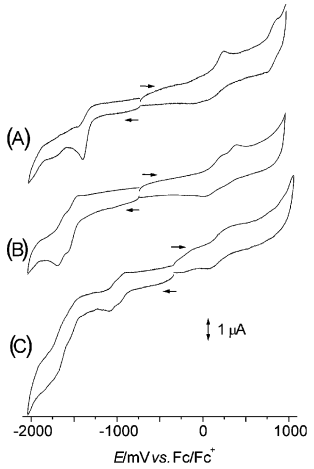

Figure 8. Cyclic voltammograms (CH_2Cl_2, 0.1 M TBAP) of **4** (A), dimeric complex **3** (B), and its bisprotonated form [**3**$(HTFA)_2$] (C).

Table 1. Anodic (E_a) and Cathodic (E_c) Peak Potentials of the Redox Couples in Cyclovoltammograms Recorded for **3** and **4** in CH_2Cl_2

	oxidation		reduction	
complex	E_a	E_c	E_a	Ec
3	210	55	−1476	−1554
	420	80	−1630	−1700
3a	190	25	−1467	−1542
	385	300	−1620	−1690
4	235	109		−1405
	835	776		
[**3**$(HTFA)_2$]	340	100	−897	−962
			−997	−1063

wave potentials of which differ by more than 200 mV (Figure 8B). These features indicate a strong cathodic shift of the second reduction and considerable anodic shift of the second oxidation potentials because of an electrostatic interaction between the subunits after addition/abstraction of the electron. This observation is in agreement with the two-stage chemical oxidation of **3** described above for the spectrophotometric titration with bromine. For the reference monomeric complex **4**, there is only one reduction and one oxidation process observed in the respective potential ranges (Figure 8A).

Upon protonation of **3** with an excess of TFAH (Figure 8C), the HOMO−LUMO gap, represented here by the separation of the first reduction and first oxidation potentials, decreases by about 500 mV with respect to that of the unprotonated species. It reflects a higher tendency of the positively charged system to accept an additional electron. On the other hand, such a strong anodic shift can be related to the change of the reduction site from the ligand in **3** to the metal ion in its diprotonated form [**3**$(TFAH)_2$]. As it was in the case of the unprotonated dimer, the reduction wave is split into two reversible couples indicating stepwise addition of electrons and, thus, interaction between the subunits also in their protonated forms. However, the oxidation processes in the case of [**3**$(TFAH)_2$] are represented by only one broad, unresolved, and irreversible wave appearing at the potential close to the mean value of the two oxidation potentials observed for **3**.

The differences of the oxidation/reduction potentials of the consecutive steps of electron removal/addition arise from the Coulombic interaction between the redox centers, but they can be also interpreted in terms of the relative stability of a "mixed valence" species.[70,71] In general, the processes that occur in the system can be represented as follows

$$\mathrm{Ox{-}Ox} + \mathrm{e}^- \rightleftarrows \mathrm{Ox{-}Red}\ (E_1)$$

$$\mathrm{Ox{-}Red} + \mathrm{e}^- \rightleftarrows \mathrm{Red{-}Red}\ (E_2)$$

$$\mathrm{Ox{-}Ox} + \mathrm{Red{-}Red} \rightleftarrows 2\mathrm{Ox{-}Red}\ (K_{com})$$

where E_1 and E_2 are formal potentials of the consecutive redox processes and K_{com} is an equilibrium constant for a comproportionation reaction reflecting stability of the mixed-valence species. The difference of potentials, $\Delta E = E_2 - E_1$, is related to K_{com} by eq 1

$$\Delta E = 0.059 \log K_{com} \qquad (1)$$

A value of $K_{com} = 4$ (equivalent with $\Delta E = 35$ mV) is assumed for a purely statistic case where no interaction between the redox centers takes place, while the lower values indicate instability of the mixed-valence species. For $K_{com} \gg 4$ the monooxidized or monoreduced compound is expected to be stable. Thus, the value of $K_{com} = 3625$

(70) Gagne, R. R.; Spiro, C. L.; Smith, T. J.; Hamann, C. A.; Thies, W. R.; Shiemke, A. K. *J. Am. Chem. Soc.* **1981**, *103*, 4073.
(71) Gagne, R. R.; Koval, C. A.; Smith, T. J.; Cimolino, M. C. *J. Am. Chem. Soc.* **1979**, *101*, 4571.

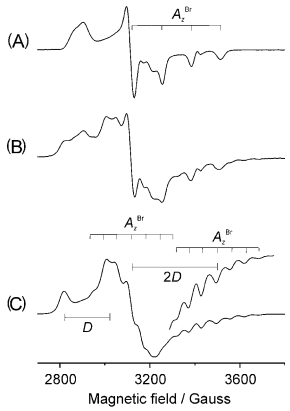

Figure 9. Selection of frozen-solution X-band EPR spectra (77 K, CH_2Cl_2) taken upon a titration of **3** with a Br_2 solution: A, 0.9 equiv; B, 2 equiv; C, 4 equiv.

calculated for the oxidation of **3** suggests stability of the monooxidated species, although it must be taken with care since the electrochemical oxidation processes are irreversible. For the reduction of **3**, the comproportionation constant is significantly lower ($K_{com} = 362$), but a mixed-valence species generated upon reduction of [**3**$(TFAH)_2$] for which $K_{com} = 68$ seems to be even less stable toward disproportionation.

An EPR-controlled titration of **3** with Br_2 allows spectroscopic identification of the chemically oxidized species. At lower bromine concentrations, an orthorhombic signal typical of d^7 nickel(III) complexes of NCP derivatives with one apical bromide ligand dominates the frozen solution EPR spectrum (CH_2Cl_2, 77 K), which is presented in the Figure 9A. The spectral parameters of **3**Br ($g_x = 2.358$, $g_y = 2.150$, $g_z = 2.062$, $A_x^{Br} = 15$, $A_y^{Br} = 35$, $A_z^{Br} = 129$ G) are similar to those obtained for the 21-benzyl-substituted derivative of nickel(III) NCP complex with bromide ligand.[28] Such a spectral pattern is typical for a predominantly d_z^2 metal-orbital contribution to the singly occupied molecular orbital (SOMO) and indicates metal-centered oxidation of **3**. Further addition of Br_2 to the solution of **3** results in a gradual appearance of another signal, which eventually replaces that of one-electron oxidized species **3**Br. The spectral pattern of this new signal (Figure 9C) indicates zero-field splitting resulting from an interaction of two electronic spins, an orthorhombic symmetry ($g_x = 2.328$, $g_y = 2.195$, $g_z = 2.065$, $D = 0.0173$ cm^{-1}, $E = -0.0018$ cm^{-1}), and a coupling with two bromine nuclei represented by two seven-line sets ($A_z^{Br} = 63$ G). The spin-Hamiltonian parameters here are those of the best-fit computer simulated spectrum calculated for an electronic spin $S = 1$ and two equivalent nuclear spins $I = 3/2$. Significantly, the value of the hyperfine tensor principal component A_z^{Br} in the spectrum of bis-oxidized species **3**Br_2 is about half of that observed for the mixed-valence complex **3**Br. Such a decrease of the hyperfine constant is typical for the systems with zero-field splitting.[72,73] No low-field "$\Delta M_s = 2$" transition is observed for **3**Br_2. The addition of **3** to the solution of bis-oxidized complex **3**Br_2 resulted in the reappearance of the spectrum diagnostic for the mixed-valence species **3**Br. This comproportionation process, indicating relatively high stability of the mixed-valence species, is expected on the basis of the electrochemical observations (vide supra).

The oxidation products were concurrently characterized by ESI mass spectrometry. For the solution containing the mono-oxidized species, the molecular ion peak of **3** (1556 amu) is accompanied by a signal at 1636 amu in agreement with the composition of **3**Br. Both these signals are still present in a mass spectrum recorded for the solution containing bisoxidized species, but a new peak appearing at 1718 amu indicates the formation of the complex consisting of two bromide ligands, that is, **3**Br_2. Under electrospray ionization conditions, the oxidized species undergo decomposition since in both mass spectra the fragmentation peaks appear at 831 and 726 amu representing the 21-xylene-substituted and unsubstituted monomeric nickel complexes of NCP, respectively. It suggests bond cleavage between coordinated C21 and the benzylic carbon similar to that observed under oxidative conditions for benzyl- or allyl-substituted complexes.[28,53]

An attempt can be made for bisoxidized species **3**Br_2 to rationalize the value of zero-field splitting in terms of the D parameter dependence on the distance between paramagnetic centers. For a purely dipolar interaction, general eq 2 provides a relationship between zero-field splitting value and the geometry of the system of interacting centers[72]

$$D = 3/4(g\beta_e)^2 < (r^2 - 3Z^2)r^{-5} > \qquad (2)$$

where g is a Zeeman principal value that is coaxial with the principal value of tensor **D**, β_e is a Bohr magneton, r is the mean distance between the two electrons with parallel spins, and Z is a component of the interelectron vector expressed in the principal-axis system. The geometric factors can be taken from the crystal structure of **3** for a rough approximation of distances and angular dependencies considering the semirigid character of the xylene bridge. With the z axis normal to the molecular macrocyclic planes of the subunits in **3**, the dependence takes a form of the eq 3

$$D = 3/4(g\beta_e)^2 < (1 - 3\cos^2\Theta)r^{-3} > \qquad (3)$$

where Θ is an angle between the axis connecting two metal centers and the principal z axis. With $r = 5.77$ Å and $\Theta = 34°$, an unrealistic low value of 0.0055 cm^{-1} for $|D|$ is obtained from eq 3. In fact, the observed value of the zero-field splitting (0.0173 cm^{-1}) suggests a much shorter distance between the paramagnetic centers that can be calculated from eq 3 as $r = 4.31$ Å for $\Theta = 0°$. Although the rotational freedom on the xylene bridge allows the totally eclipsed conformation where $\Theta = 0°$, the closest distance between the nickel centers can be estimated from a molecular model as not lower than 4.92 Å. Moreover, it is rational to anticipate an even larger distance upon coordination of bromide to each of the metal centers. Thus, it seems that relationship 2 gives a rather bad approximation of the zero-field splitting

(72) Weil, J. A.; Bolton; J. R.; Wertz, J. E. *Electron Paramagnetic Resonance. Elementary Theory and Practical Applications*; John Wiley & Sons: New York, 1994.
(73) Collman, J. P.; Elliott, C. M.; Halbert, T. R.; Tovrog, B. S. *Proc. Natl. Acad. Sci. U.S.A.* **1977**, *74*, 18.

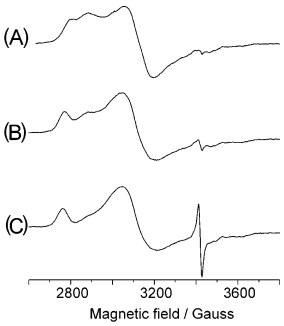

Figure 10. Selected frozen solution EPR spectra (X-band, CH_2Cl_2, 77 K) taken upon titration of [**3**$(HBr)_2$] (complex **3** acidified with a 4-fold molar excess of HBr solution in acetic acid) with bromine (solution in CH_2Cl_2): A, 0.5 equiv; B, 1.4 equiv; C, 4 equiv of Br_2.

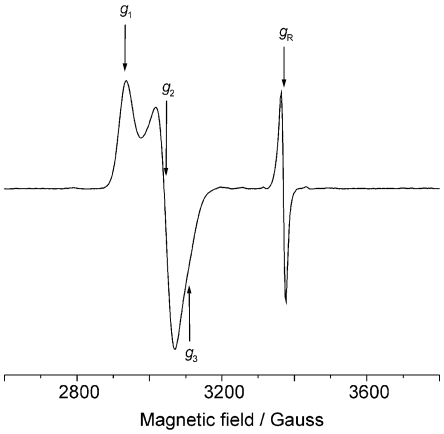

Figure 11. Frozen solution EPR spectrum (X-band, CH_2Cl_2, 77 K) of the product of reduction of **3** with $N_2H_6Cl_2$. The signal of free radical that is concurrently formed is observed at $g_R = 2.003$.

parameter in the case of **3**Br_2. The reason for the higher than expected value of D could be the contribution of some pseudo-dipolar interaction between the paramagnetic centers that involves the bridging phenylene ring. The conformational space of **3** includes an eclipsed arrangement of the subunits with the phenylene ring lying between macrocyclic planes in a close distance of about 2.3 Å from both metal centers. That may facilitate communication between the subunits influencing both redox properties and electronic interaction in the system.

Under acidic conditions, both oxidation and reduction products can be detected by EPR in a frozen CH_2Cl_2 solution. The addition of bromine to the solution of **3** acidified with HBr results in the appearance of a rather broad signal centered at $g = 2.18$ accompanied by weaker features at $g = 2.44$ and $g = 2.37$ and a sharp radical line at $g = 2.003$ which is often encountered upon oxidation/reduction of porphyrin species (Figure 10). The intensity ratio of these signals depends on the concentration of Br_2; however, unlike in the case of **3**, a unique signal diagnostic for mono-oxidized species cannot be observed even at substoichiometric amounts of bromine. It can reflect the small difference between first and second oxidation potentials in [**3**$(HX)_2$] and, thus, the relative instability of the mixed-valence species. It should also be pointed out that because of the triplet spin state of an unoxidized part of the dimer the spectrum of the monooxidized species under acidic conditions can be considerably different from that of **3**Br. The spectrum obtained upon addition of an excess of Br_2 is characterized with similar spin-Hamiltonian parameters as in the case of $3Br_2$ except for the hyperfine splitting, and thus a similar interaction of the paramagnetic centers can be assumed in both systems. The addition of a noncoordinating base (2,4,6-collidine) to the solution of the fully oxidized complex resulted in the appearance of a signal identical to that observed for **3**Br_2, indicating deprotonation of the external nitrogens of the confused pyrroles.

Scheme 2

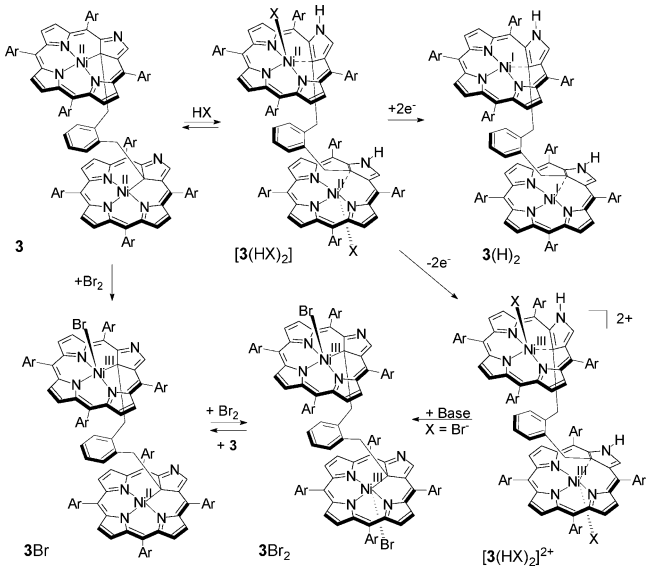

The reduction of **3** under acidic conditions can be accomplished with hydrazine dihydrochloride. The reaction was carried out by means of $N_2H_6Cl_2$ dissolved in a DMF/H_2O mixture (10:1) that was shaken with a deaerated CH_2Cl_2 solution of **3**. The resulting EPR spectrum of frozen solution (77 K) consists of a signal that is almost identical with that obtained previously for monomeric 21-alkylated nickel complexes of NCP reduced with the same agent.[28] The spin-Hamiltonian parameters ($g_1 = 2.298$, $g_2 = 2.218$, $g_3 = 2.192$) indicates some rhombic distortion, but the spectrum does not involve any features that could be assigned to the presence of the two interacting paramagnetic centers (Figure 11). This result suggests either a reduction of only one nickel(II) ion in [**3**$(HCl)_2$] or lack of interaction between the paramagnetic centers in the bisreduced species. The latter is in agreement with relatively low value of K_{com} for this process, calculated based on the separation of reduction potentials (vide supra) and the expected low stability of the mixed-valence species. Nevertheless, the spectral parameters, that is, pronounced anisotropy of the Zeeman tensor indicate a metal-centered reduction that yields nickel(I) species as suggested on the basis of the reduction potential values for the protonated complex. For the monovalent nickel of electronic configuration d^9, the contribution of the $d_{x^2-y^2}$ metal orbital to the SOMO can be predominant,[74,75] which may

(74) Chmielewski, P. J.; Grzeszczuk, M.; Latos-Grażyński, L.; Lisowski, J. *Inorg. Chem.* **1989**, *28*, 3546.
(75) Chmielewski, P. J.; Latos-Grażyński, L.; Pacholska, E. *Inorg. Chem.* **1994**, *33*, 1992.

Table 2. Crystal Data and Structure Refinement for 3•(CH_2Cl_2)(*n*-hexane)

empirical formula	$C_{112}H_{89}Cl_4N_8Ni_2$
fw	1806.13
temp	100(2) K
wavelength	1.54178 Å
cryst syst	triclinic
space group	$P\bar{1}$
unit cell dimensions	
a	16.455(3) Å
b	16.776(3) Å
c	18.400(4) Å
α	77.43(3)°
β	75.31(3)°
γ	66.20(3)°
vol	4457.1(19) Å^3
Z	2
density (calcd)	1.346 Mg/m^3
abs coeff (Cu Kα)	2.064 mm^{-1}
F(000)	1882
cryst size	0.3 × 0.2 × 0.15 mm^3
crystal color and habit	black block
diffractometer	Oxford Diffraction Xcalibur PX
θ range	3.5−60.0°
index ranges	$-18 \le h \le 18$, $-18 \le k \le 18$, $-13 \le l \le 20$
reflns collected	24 566
independent reflns (R_{int})	12 274 (0.081)
abs correction	analytical
max and min transm	0.8560 and 0.8174
solution method	direct
refinement method	full-matrix least-squares on F^2
data/restraints/params	6502/6/1111
GOF on F^2	1.012
final R indices [$I > 2\sigma(I)$][a]	R1 = 0.0903, wR2 = 0.2308
R indices (all data)[a]	R1 = 0.1378, wR2 = 0.2732
largest diff peak and hole	0.98 and −0.76 e•Å^{-3}

[a] $R1 = \sum||F_o| - |F_c||/\sum|F_o|$, $wR2 = [\sum[w(F_o^2 - F_c^2)^2/\sum[w(F_o^2)^2]]^{1/2}$.

reduce the interaction between the unpaired spins in the face-to-face-arranged dimers in contrast to the bis(nickel(III)) complexes where an "axial" d_{z^2} metal orbital is involved in the singly occupied molecular orbital in each subunit. The change of the arrangement of the subunits with respect to each other upon the protonation/reduction that results in an unfolded conformation of the dimer where the subunits are no longer cofacial can also be taken into account.

Scheme 2 summarizes redox properties observed for **3** and its protonated form.

Conclusion

The structural, nucleophilic, and redox properties of the 21,21′-xylene-linked bis(NCP nickel(II)) complex resemble to some extent those of the monomeric analogues,[27−29] although cooperative effects caused by the dimeric character of **3** are evident. The interaction between the subunits can be observed despite isolation of their aromatic *π*-electron systems. The diversity of the oxidation and spin states that the system can adopt is important for potential applications in molecular electronics. The nucleophilic sites on the perimeter of each of the subunits allow modification of the redox properties by protonation. Since the outer nitrogen of the confused pyrrole has been shown to coordinate metal ions in several systems[15,16,18−20,22,24,33,54] including those of 21-alkylated nickel(II) NCP complexes,[53] dimer **3** possessing two such donors can be exploited for a preparation of coordinatively linked oligomeric assemblies comprising of **3** as a "conducting" bridge.

Experimental Section

Instrumentation. Absorption spectra were recorded on a diode array Hewlett-Packard 8453 spectrometer. Mass spectra were recorded on an AD-604 spectrometer using the electrospray technique. NMR spectra were recorded on a Bruker Avance 500 spectrometer. The 1D and 2D experiments (COSY, NOESY, HMQC, and HMBC) were performed by means of standard experimental procedures of the Bruker library. The peaks were referenced to the residual $CHCl_3$ resonances in ^{1}H and ^{13}C NMR (7.24 and 77.2 ppm, respectively). Cyclovoltammetric measurements were performed in dichloromethane on an EA9C MTM apparatus with a glassy carbon disk as the working electrode, Ag/AgCl as the reference electrode (ferrocene reference potential was 530 mV), and platinum wire as the auxiliary electrode. Tetrabutylammonium perchlorate (0.1 M) was used as the supporting electrolyte. EPR spectra were obtained with a Bruker ESP 300E spectrometer. The magnetic field was calibrated with a proton magnetometer and EPR standards. The EPR spectra were simulated by assuming orthorhombic symmetry by means of WINEPR SimFonia computer program.

Preparation of Precursors. 5,10,15,20-Tetrakis(*p*-tolyl)-2-aza-21-carbaporphyrin (**1**) and its nickel(II) complex (**2**) were synthesized according to known procedures.[1,3]

Synthesis of Dimer 3. In a typical synthesis, 30 mg (0.041 mmol) of 5,10,15,20-tetrakis(*p*-tolyl)-2-aza-21-carbaporphyrinato nickel(II) **2** and 20 mg (0.075 mmol) of 1,2-bis(bromomethyl)-benzene were dissolved in CH_2Cl_2 (30 mL). A suspension of K_2CO_3 (20 mg) in ethanol (10 mL) was added to the solution, and the mixture was stirred for 12 h at room temperature in darkness. Flash chromatography on silica gel with CH_2Cl_2 that was eventually replaced with a CH_2Cl_2/EtOH mixture (5% of ethanol) allows the separation of reaction product **3** from the residual starting material **2** (fastest migrating green band) and monomeric product of alkylation **4** (second reddish band migrating with 2% EtOH). Yields (crystallization from CH_2Cl_2/hexane): **3**, 19 mg, (60%); **4**, 10 mg, (23%). Selected data for **3**. UV−vis (CH_2Cl_2) *λ*/nm ($\epsilon \times 10^{-3}$): 247 sh, 290 (65), 363 (75), 434 (118), 462 sh, 612 sh, 772 sh. ^{1}H NMR (500 MHz, $CDCl_3$, 298 K): *δ* 8.74 (s, 1H), 8.60 (s, 1H), 8.34 (d, ^3J = 4.6 Hz, 1H), 8.33 (d, ^3J = 4.2 Hz, 1H), 8.30 (d, ^3J = 4.6 Hz, 1H), 8.29 (d, ^3J = 4.3 Hz, 1H), 8.12 (d, ^3J = 4.8 Hz, 1H), 7.98 (d, ^3J = 4.6 Hz, 1H), 7.86 (b, 1H), 7.71 (b, 2H), 7.69 (d, ^3J = 4.2 Hz, 1H), 7.58 (b, 2H), 7.54 (b, 2H), 7.51 (d, ^3J = 7.6 Hz, 2H), 7.38 (d, ^3J = 8.0 Hz, 1H), 7.36 (d, ^3J = 4.2 Hz, 1H), 7.28 (d, ^3J = 4.2 Hz, 1H), 7.22 (b, 4H), 7.05 (d, ^3J = 7.8 Hz, 2H), 6.91 (m, 1H), 6.89 (m, 1H), 6.75 (d, ^3J = 7.1 Hz, 2H), 6.66 (d, ^3J = 4.3 Hz, 1H), 5.55 (m, 1H), 5.52 (m, 1H), 2.79 (s, 3H), 2.76 (s, 6H), 2.74 (s, 3H), 2.49 (s, 3H), 2.43 (s, 3H), 2.40 (s, 3H), 2.35 (s, 3H), −2.85 (d, ^2J = 15.1 Hz, 1H), −2.95 (d, ^2J = 14.9 Hz, 1H), −3.03(d, ^2J = 14.9 Hz, 1H), −3.26 (d, ^2J = 15.1 Hz, 1H). ^{13}C NMR (126 MHz, $CDCl_3$, 298 K): *δ* 177.1, 176.8, 155.8, 155.6, 155.3, 155.1, 152.7, 152.5, 152.3, 151.9, 149.9, 149.7, 149.0, 148.8, 147.3, 147.2, 146.7, 146.5, 138.3, 138.1, 138.0, 137.9, 137.9, 137.6, 137.5, 137., 137.4, 137.4, 136.6, 136.6, 136.3, 136.2, 135.6, 135.6, 135.5, 135.3, 135.2, 134.3, 134.3, 133.5, 133.0, 132.3, 132.3, 132.1, 131.9, 131.5, 131.4, 131.0, 130.9, 130.7, 130.0, 129.4, 128.4, 128.4, 128.2, 128.1, 127.8, 127.7, 127.2, 126.7, 125.8, 125.7, 125.1, 124.9, 123.9, 123.8, 122.4, 122.3, 40.0, 39.9, 29.3, 21.7, 21.7, 21.6, 21.4, 21.3, 21.2. MS (ESI): *m*/*z* 1556.8 (obsd), 1557.2 (calcd for $C_{104}H_{78}N_8Ni_2$).

The same procedure was applied for the synthesis of **3a** except that the 5,10,15,20-tetraphenyl-2-aza-21-carbaporphyrinato nickel-

(II) was used instead of tetratolyl derivative as the starting NCP nickel(II) complex **2**. Selected data for **3a**. ^{1}H NMR (500 MHz, $CDCl_3$, 298 K): δ 8.79 (s, 1H), 8.65 (s, 1H), 8.34 (d, ^3J = 4.9 Hz, 1H), 8.33 (d, ^3J = 4.9 Hz, 1H), 8.30 (d, ^3J = 4.9 Hz, 2H), 8.10 (d, ^3J = 4.9 Hz, 1H), 7.96 (d, ^3J = 4.2 Hz, 1H), 7.93 (b, 1H), 7.85 (d, ^3J = 7.9 Hz, 1H), 7.81 (d, ^3J = 6.1 Hz, 1H), 7.80 (d, ^3J = 8.5 Hz, 1H), 7.78 (d, ^3J = 7.3 Hz, 1H), 7.76 (b, 3H), 7.72 (d, ^3J = 7.3 Hz, 2H), 7.70 (d, ^3J = 7.3 Hz, 2H), 7.68 (d, ^3J = 4.9 Hz, 2H), 7.66 (d, ^3J = 6.1 Hz, 1H), 7.59 (d, ^3J = 7.3 Hz, 2H), 7.57 (d, ^3J = 7.3 Hz, 2H), 7.53 (d, ^3J = 7.3 Hz, 1H), 7.48 (d, ^3J = 7.3 Hz, 1H), 7.44 (d, ^3J = 7.3 Hz, 2H), 7.42 (b, 3H), 7.39 (d, ^3J = 7.3 Hz, 1H), 7.34 (b, 2H), 7.32 (d, ^3J = 7.9 Hz, 2H), 7.27 (t, ^3J = 7.3 Hz, 2H), 7.23 (d, ^3J = 4.9 Hz, 1H), 6.95 (m, 1H), 6.93 (m, 1H), 6.88 (d, ^3J = 6.7 Hz, 2H), 6.76 (d, ^3J = 4.9 Hz, 1H), 5.56 (m, 1H), 5.54 (m, 1H), −2.87 (d, ^2J = 15.2 Hz, 1H), −2.99 (d, ^2J = 15.2 Hz, 1H), −3.06 (d, ^2J = 15.2 Hz, 1H), −3.31 (d, ^2J = 15.2 Hz, 1H). ^{13}C NMR (126 MHz, $CDCl_3$, 298 K): δ 176.9, 176.7, 155.9, 155.8, 155.5, 155.3, 155.3, 152.8, 152.8, 152.6, 152.4, 149.8, 149.7, 149.6, 148.9, 148.7, 147.3, 147.1, 147.0, 146.6, 146.4, 141.7, 141.1, 140.8, 140.7, 140.6, 140.6, 140.4, 140.3, 139.9, 139.6, 139.3, 138.9, 138.8, 138.7, 138.5, 136.7, 136.3, 135.5, 135.4, 135.1, 134.3, 134.1, 133.7, 133.1, 132.4, 132.3, 132.3, 132.1, 132.0, 131.6, 131.5, 131.1, 130.8, 130.1, 129.7, 129.5, 129.2, 129.1, 128.3, 128.2, 127.8, 127.7, 127.6, 127.5, 127.4, 127.3, 127.2, 127.0, 125.4, 125.2, 125.1, 123.9, 123.9, 122.6, 122.5, 39.6, 39.4, 31.5. MS (ESI): *m*/*z* 1444.3 (obsd), 1444.9 (calcd for $C_{96}H_{62}N_8Ni_2$).

X-ray Data Collection and Refinement of 3. Crystals of **3**·$(CH_2Cl_2)_2$(*n*-hexane) were prepared by diffusion of *n*-hexane into the dichloromethane solution in a thin tube. Data were collected at 100 K using an Oxford Cryosystem device on an Oxford Diffraction Xcalibur PX diffractometer with KM4CCD Sapphire detector. Data collection, integration and scaling of the reflections, and analytical absorption correction were performed by means of the CrysAlis suite of programs (Oxford Diffraction, Poland). Crystal data are compiled in Table 2. The structure was solved by direct methods with SHELXS97[76] and refined by the full-matrix least-squares method on all F^2 data using SHELXL97[77] programs. All non-H atoms were refined with anisotropic displacement parameters; hydrogen atoms were included from the geometry of molecule. The asymmetric unit contains **3**, two disordered molecules of dichloromethane, and one molecule of hexane disordered onto two sites.

Synthesis of (5,10,15,20-Tetrakis(*p*-tolyl)-21-(2′-bromomethylphenylmethylene)-2-aza-21-carbaporphyrinato)nickel(II) (4). A mixture of **2** (30 mg, 0.041 mmol) and 1,2-bis(bromomethyl)-benzene (16 mg, 0.061 mmol) in dichloromethane solution (50 mL) containing 2 mg of dibenzo-18-crown-6 and a suspension of K_2CO_3 (10 mg) was refluxed for 2 h under a blanket of nitrogen. The solvent was evaporated under reduced pressure. The solid was dissolved in dichloromethane and chromatographed on a silica gel column. The second brown-reddish band that contained **4** was eluted with dichloromethane/ethanol (2% EtOH) and crystallized from a CH_2Cl_2/hexane mixture. Yield: 21 mg (57%). Selected data for **4**. UV−vis (CH_2Cl_2) λ/nm ($\epsilon \times 10^{-3}$): 242 sh, 291 (32), 364 (40), 437 (62), 464 sh, 611 sh, 779 sh.^{1}H NMR (500 MHz, $CDCl_3$, 298 K): δ 9.46 (s, 1H), 8.66 (d, ^3J = 4.6 Hz, 1H), 8.63 (d, ^3J = 4.6 Hz, 1H), 8.53 (d, ^3J = 4.6 Hz, 1H), 8.51 (d, ^3J = 4.6 Hz, 1H), 8.47 (d, ^3J = 4.3 Hz, 1H), 8.43 (d, ^3J = 4.3 Hz, 1H), 8.04 (b, 1H), 7.95 (b, 3H), 7.84 (b, 1H), 7.74 (d, ^3J = 7.8 Hz, 2H), 7.54 (d, ^3J = 7.6 Hz, 2H), 7.50 (d, ^3J = 7.4 Hz, 4H), 7.00 (t, ^3J = 7.4 Hz, 1H), 6.92 (t, ^3J = 7.2 Hz, 1H), 6.78 (d, ^3J = 7.6 Hz, 1H), 5.81 (d, ^3J = 7.6 Hz, 1H), 2.90 (d, ^2J = 10.3 Hz, 1H), 2.64 (s, 6H), 2.60 (s, 3H), 2.59 (d, ^2J = 10.3 Hz, 1H), 2.58 (s, 3H), −0.72 (d, ^2J = 15.1 Hz, 1H), −1.3 (d, ^2J = 15.1 Hz, 1H). MS (ESI): *m*/*z* 911.2 (obsd), 911.2 (calcd for $C_{56}H_{43}N_4Ni + H^+$).

Synthesis of (5,10,15,20-Tetrakis(*p*-tolyl)-2,21-bis(2′-bromomethylphenylmethylene)-2-aza-21-carbaporphyrinato)nickel(II) Bromide (5). A mixture of **2** (30 mg, 0.041 mmol) and 1,2-bis-(bromomethyl)benzene (40 mg, 0.15 mmol) in dichloromethane solution (50 mL) containing 2 mg of 18-crown-6 and a suspension of K_2CO_3 (10 mg) was refluxed for 8 h under a blanket of nitrogen. The solvent was evaporated under reduced pressure. The solid was dissolved in dichloromethane and chromatographed on a silica gel column. The third brown-reddish band that contained **5** was eluted with dichloromethane/ethanol (5% EtOH) and crystallized from a CH_2Cl_2/hexane mixture. Yield: 27 mg (57%). Selected data for **5**. UV−vis (CH_2Cl_2) λ/nm ($\epsilon \times 10^{-3}$): 314 (26), 370 (28), 430 sh, 469 (41), 590 (8), 644 (9), 741 (11), 852 sh. ^{1}H NMR (500 MHz, $CDCl_3$, 298 K): δ 67.5, 65.1, 59.6, 55.5, 50.3, 49.0, 35.2, 32.2, 26.8, 25.2, 10.8, 10.5, 9.8, 9.3, 8.6, 8.0, 7.8, 7.6, 7.5, 6.8, 6.6, 6.0, 5.8, 4.9, 4.7, 4.5, 4.3, 4.0, 3.5, 2.5, 2.4, 2.2, 1.9, −1.6. MS (ESI): *m*/*z* = 1174.5 (obsd), 1174.5 (calcd for $C_{64}H_{51}N_4NiBr_3$).

Acknowledgment. This work was supported by the Ministry of Scientific Research and Information Technology of Poland under Grant 3 T09A 162 28.

Supporting Information Available: Crystallographic data of **3** in CIF format, 2D NMR spectra for **3**, **3a**, and **4**, and spectrophotometric titration of **3** and **4** with TFAH. This material is available free of charge via the Internet at http://pubs.acs.org.

IC061793E

(76) Sheldrick, G. M. *SHELXS97, Program for Crystal Structure Solution*; University of Göttingen: Göttingen, Germany,1997.
(77) Sheldrick, G. M. *SHELXL97, Program for Crystal Structure Refinement*; University of Göttingen: Göttingen, Germany, 1997.